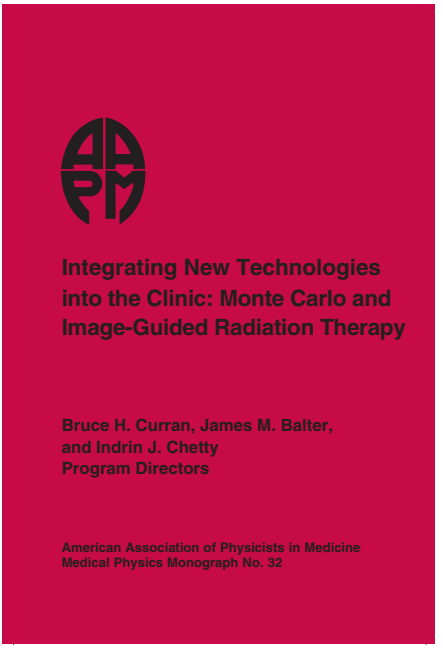

Here is a sample chapter from this book.

Monte Carlo Non-Adaptive 4-D Treatment Planning in Conformal Radiation Therapy: Why, How, and What To Look For

Mihaela Rosu, Ph.D., Indrin J. Chetty, Ph.D., Marc L. Kessler, Ph.D., and Randall K. Ten Haken, Ph.D.
Department of Radiation Oncology, University of Michigan, Ann Arbor, Michigan

Introduction and Scope 293
Dose Accumulation in 4-D Treatment Planning 296
How Much 4-D Information Is Needed for Planning? 299
Image Registration—Where It Matters the Most 300
Motion/Deformation vs. Heterogeneity Effects 304
Conclusions 306
Acknowledgment 307
References 307

Introduction and Scope

The term "motion" is quite broad in radiation therapy and can refer to setup inaccuracies, displacements due to respiration or other physiological movements (peristaltic, cardiac-related), and deformations (such as those induced by breathing or tumor shrinkage). In this chapter "motion" will be used in a narrower sense, specifically, in relation to the displacements and the deformations that occur as a result of breathing.

The undesired effects of breathing are apparent from the very first step in the radiation therapy planning process, during imaging. A dataset acquired under free breathing has artifacts (Balter et al. 1996; Wong et al. 1999; Shimizu et al. 2000) that make target delineation inaccurate. Furthermore, even if respiratory motion at the time of imaging is limited by employing techniques such as active breathing control (Wong et al. 1999; Dawson et al. 2001) or breath hold (Hanley et al. 1999; Rosenzweig et al. 2000; Mah et al. 2000), the three-dimensional (3-D) description of the patient's geometry represents only one instance of an anatomy that is otherwise changing on a time scale shorter than the time required to deliver one treatment fraction. As a consequence, a treatment designed by using such a dataset inaccurately describes the dose to be received by a patient during treatment, since the patient displacements with respect to the planned treatment beams and the changes in tissue density that occur during respiration are not accounted for prior to treatment delivery. The need to circumvent such problems, especially in an era when treatment margins become tighter and plans more and more conformal, led to the onset of a new approach—four-dimensional (4-D) imaging, in which multiple datasets are acquired over various segments of the breathing cycle (Vedam et al. 2003; Low et al. 2003; Pan et al. 2004; Keall et al. 2004).

The philosophy of designing 4-D treatments is similar to the one employed in 3-D planning in the sense that the overall goal is to maximize the therapeutic ratio by delivering as much dose as possible to the tumor, while sparing normal tissues and organs at risk (Fraass 1995). However, while the assessment of the dose to be delivered in 4-D is still performed on a single dataset, often called the "planning dataset" (PD), the dose reported now represents an accumulation of the doses received during the various phases of the breathing cycle.

The question then is how one could make best use of the abundance of time-dependent anatomical information gathered during imaging when designing the treatment plans. The answer depends on whether the same treatment plan or different plans will be delivered at various phases of the breathing cycle. We will use the term "non-adaptive delivery" for the former approach, whereas the latter one is usually referred to as "adaptive delivery." The flow of the events during the treatment planning is schematically shown in Figure 1 for both strategies.

In the case of non-adaptive delivery, first the target and other structures of interest are defined on the chosen PD. Then a plan is designed on the PD and dose distributions are re-computed on several datasets at various phases in the breathing cycle using this plan. The last step is the accumulation (Keall et al. 2004; Schaly et al. 2004; Rietzel et al. 2005; Brock et al. 2003; Rosu et al. 2005; Heath and Seuntjens 2006) of these doses and scoring them back on the PD. The dose accumulation is accomplished by using image registration techniques (Bookstein 1989; Violla and Welles 1995; Rueckert et al. 1999; Kessler et al. 2004; Kessler and Roberson 2005) that provide non-rigid body voxel mapping between datasets acquired over various segments of the ventilatory cycle. The beam number, weights, and directions are then manipulated until the cumulative dose provides the desired target coverage and normal tissue sparing. This approach is technically 4-D only during the imaging segment. However, it is superior to a purely 3-D planning because it estimates with increased accuracy the doses that will actually be received by tumor and normal tissues during free breathing delivery.

In a more sophisticated approach, separate plans can be designed on each available dataset with the intent of achieving the desired target coverage at each breathing phase. This implies that the target and other structures of interest have to be first segmented on all datasets. This can be done either manually or automatically (the structures of interest are first segmented on the PD and then mapped on all other datasets using the transformation provided by the registration technique) (van Herk and Kooy 1994; Austin-Seymour et al. 1995; Ketting et al. 1997; Mazonakis et al. 2001; Keall et al. 2004; Rietzel et al. 2005; Foskey et al. 2005). The treatment beams are added first on the PD and while their directions are kept the same for all datasets, the weights are adjusted and the apertures are modified so that they conform to the target from the beam's eye view for each dataset (Keall et al. 2005). Such a treatment planning strategy is followed by an adaptive delivery, in which each plan is delivered when the patient is at the corresponding breathing phase, thus making the entire process (i.e., imaging, planning, and delivery) 4-D. Of course, the whole process is subject to the

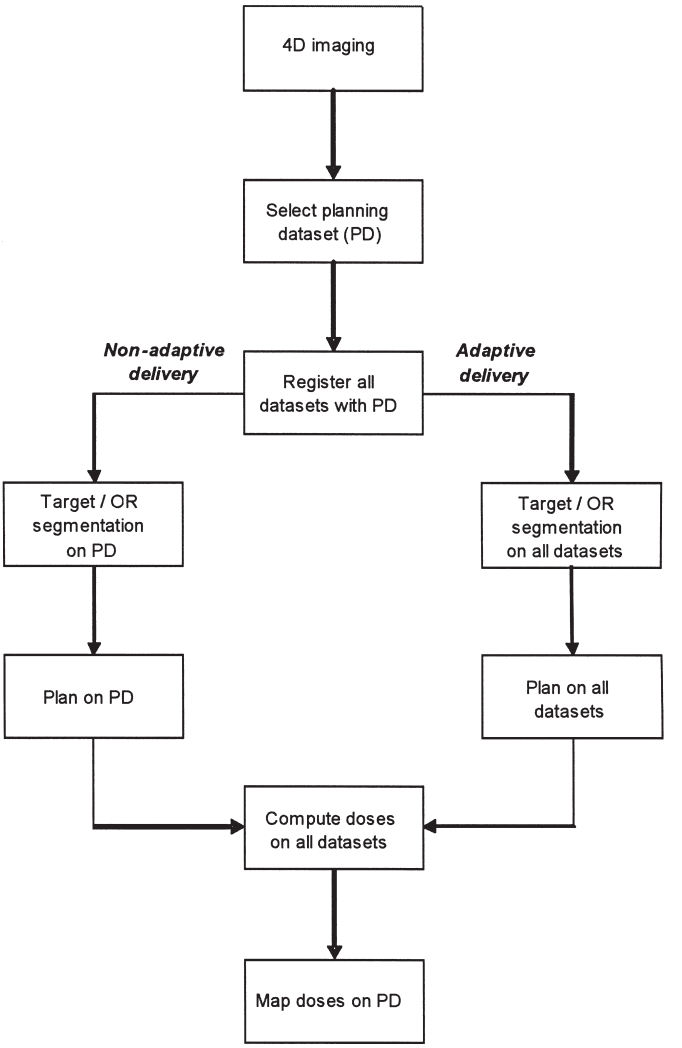

Figure 1. The flow of the events during the planning segment of a radiation therapy treatment when 4-D imaging data are available (OR = organs at risk).

constraints imposed by the ability of the treatment machine to deliver a continually adapting plan.

Regardless of the strategy adopted, the accumulation of the doses on the PD is one common segment and details on how this should be dealt with are presented below. As already mentioned, an image registration technique is required for dose accumulation. A thorough review of the registration process is beyond the scope of this chapter. However, some examples will be provided in order to illustrate where the accuracy of

the registration technique is likely to be of greater importance. Another important question that we will try to address (given the abundance of 4-D data that can be currently gathered in clinics across the country) is how much 4-D data are needed for treatment planning when a non-adaptive delivery strategy is employed.

The issues raised so far are related to how the 4-D geometrical information can/should be manipulated for treatment planning. However, the accuracy of the dose calculation algorithm remains of great importance, just as it does in 3-D planning. Here, although in the examples to follow dose calculations were performed using Monte Carlo–based calculation tools (Chetty et al. 2003), we will not try to provide arguments as to what calculation algorithm should be used for dose calculation. Instead, we will try to address the problem of how the effects due to tissue heterogeneities on one hand and motion/deformation on the other hand compare to each other.

Dose Accumulation in 4-D Treatment Planning

When dealing with deforming anatomies, the basic idea for dose accumulation from multiple datasets is to track anatomical voxels between the PD and any other available dataset (OD) using the transformation provided by the registration technique. This is necessary to obtain an estimate of the dose received at the OD by each displaced PD voxel and to accumulate this dose back onto the PD voxel (Brock et al. 2003; Keall et al. 2004; Rietzel et al. 2005; Schaly et al. 2004; Rosu et al. 2005; Heath and Seuntjens 2006). For convenience, the anatomical voxels are usually defined as the dose grid voxels from the PD, as shown in Figure 2.

In Monte Carlo–based dose calculation algorithms, the dose at each grid point is the average energy deposited in a voxel centered at the grid point. The most direct way of estimating the dose received by the PD voxel at the OD is to map the center of the PD voxel onto the OD dose grid and compute the dose at the tracked location by tri-linear interpolation of the doses at the closest neighboring dose grid points. However, when the PD voxel expands at the OD across several dose grid voxels, the dose at the tracked center might not be representative of the energy deposited in the voxel, because not all OD grid points falling within the expanded voxel are accounted for by the direct tri-linear interpolation. Therefore, the above method can be refined as follows: each PD voxel is first subdivided into octants, the center of each octant is mapped to locations on the OD dose grid, doses at tracked locations are estimated by tri-linear interpolation, and their average values are scored at the original PD dose grid point location (Rosu et al. 2005). The accumulation of doses in the deforming dataset is performed by applying time-weighting factors representing the relative amount of time spent at a particular breathing phase derived from a breathing probability distribution function:

$$D_{rec}(i) = \sum_k w_k \cdot D_k(i) \,, \tag{1}$$

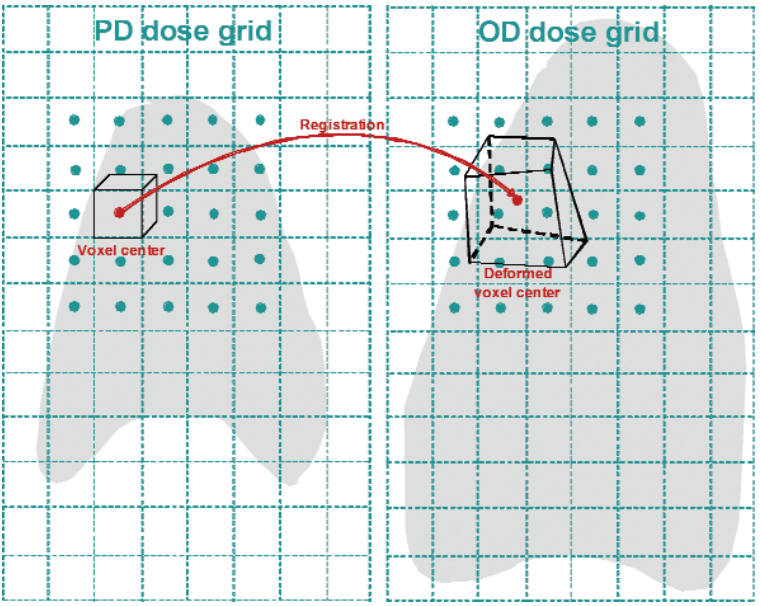

Figure 2. The accumulation of dose from multiple datasets when dealing with deforming anatomies is accomplished by tracking anatomical voxels between the planning dataset (PD) and any other dataset (OD) available using the transformation provided by a registration technique. The dose received at OD by each PD voxel is estimated and then accumulated back onto the PD voxel. For convenience, the anatomical voxels are usually defined as the dose grid voxels from the PD.

where $D_{rec}(i)$ is the cumulative dose in the PD voxel i, k the breathing phase, $D_k(i)$ the dose received by the PD voxel i at the breathing phase k, and w_k the time-weighting coefficient at breathing stage k.

Rosu et al. (2005) have shown that, when the inhale dose in the thorax is mapped back onto an exhale dataset (this being the worst-case scenario given the amount of motion and deformation occurring in the thorax), 2% to 6% point dose differences exist in the high-dose gradient regions between the direct and the refined method as the dose grid size increases from 3.5 mm to 10 mm. Figure 3(a) illustrates a dose difference map between inhale doses mapped back on the planning exhale dataset as predicted by the refined and the direct interpolation methods (±2% differences are shown here for a 3.5-mm dose grid). However, as pointed out by the University of Michigan group (Rosu et al. 2005), dose changes induced by positional and shape changes from ventilation are more significant than the errors due to an increasing dose calculation grid. As an example, Figure 3(b) shows about ±15% differences between the cumulative dose from exhale and inhale and the dose computed by using only the PD (in this case, exhale). Therefore, differences due solely to the interpolation approach used to map doses from a given dataset back on the PD are unlikely to result in clinically signifi-

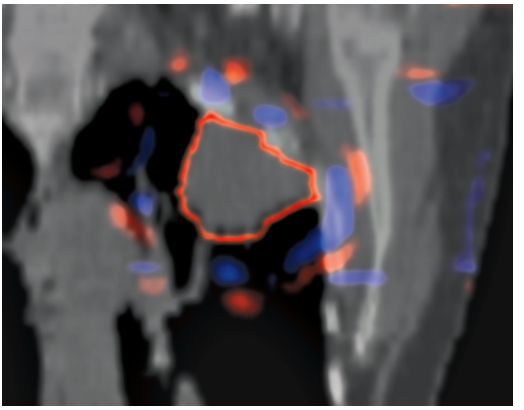

Figure 3(a). Dose difference map between inhale doses mapped back on the planning exhale dataset as predicted by the refined and the direct interpolation methods. The red/blue areas correspond to ±2% point dose differences (on a 3.5 mm dose grid size).

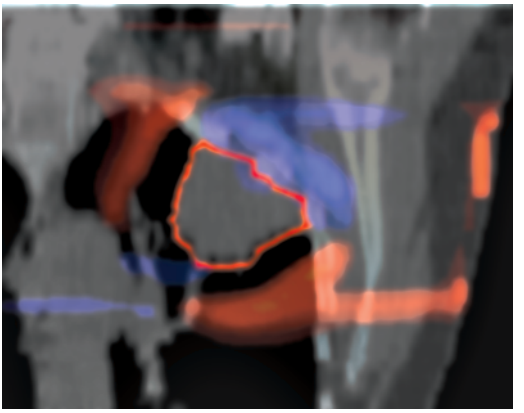

Figure 3(b). Dose difference map between the cumulative dose and the dose computed by using only the exhale planning dataset, revealing about ±15% differences. For the cumulative dose, exhale and inhale doses have been used with the appropriate time weighting coefficients (0.7 for exhale and 0.3 for inhale [Rosu et al. 2005)].

cant alterations in volume-based evaluation metrics, such as mean lung dose, normal tissue complications probability (NTCP) and tumor equivalent uniform dose (*gEUD*). It should also be pointed out that, for clinically relevant grid sizes, the use of the refined method is not necessarily equivalent to the use of the direct method at a finer grid resolution because the larger dose calculation grid inherits erroneous voxel dose estimation in the first place. In the study by Rosu et al. (2005), the change of the grid size from 3.5 mm to 10 mm did not significantly change the treatment metrics for

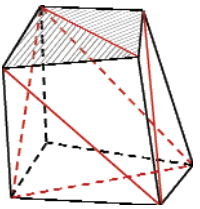

Figure 4. Nonrectangular deformed voxels are approximated by with 12 planes and used for dose tracking. [Adapted from Heath and Seuntjens (2006).]

tumors located in the thorax and for the normal lung, but led to erroneous estimates for esophagus doses when the esophagus was in the proximity of the target. This is explained by the fact that the esophagus is a serial organ and thus it is sensitive to local changes in doses, as opposed to a parallel organ such as the lung where the mean dose is known to correlate with effect. As a rule of thumb, a 3- to 4-mm dose grid size is adequate to minimize interpolation errors in dose re-mapping. The interpolation methods presented above do not explicitly account for the change in the mass of each voxel during ventilation, based on the assumption that the mass of inhaled/exhaled air is much smaller than that of the lung tissue. This is a reasonable assumption and means that mass variations can be ignored.

The use of a Monte Carlo dose calculation algorithm also allows for the calculation of the energy deposited directly in the deformed voxel, rather than calculating the energy in rectangular voxels followed by interpolation. This can be accomplished by setting the boundaries for particle transport as the deformed voxel boundaries. This approach has been recently reported by Heath and Seuntjens (2006). They have modified the DOSXYZnrc/EGSnrc user code to track dose deposition in nonrectangular voxels obtained by applying deformation vectors provided by the image registration software to the reference geometry; each deformed voxel was approximated with 12 planes as shown on Figure 4. The method of Heath and Seuntjens (2006) is approximately equivalent to that of Rosu et al. (2005) at clinically relevant grid sizes.

How Much 4-D Information Is Needed for Planning?

Ideally, the cumulative dose would have to be expressed as a time integral over all possible intermediate states between exhale and inhale, rather than a summation over a certain number of sampled states. However, this is not a practical approach, as it would require an infinite number of image datasets. Besides, since doses are always reported "per voxel," any sampling of a displacement that is finer than the dose voxel side is in fact an oversampling of the data that would bring little or no additional accuracy in the estimated cumulative dose. This leads us to the question of how many intermediate states need to actually be considered for treatment planning before the cumulative dose reaches convergence (assuming free breathing, non-adaptive

delivery). The issue has been recently addressed in a study by Rosu et al. (2006) who have compared cumulative doses estimated in several scenarios by considering: (1) only the exhale and inhale geometries ("2-state dose"); (2) the average breathing phases from the first and the second half of the time interval between exhale and inhale ("2-ave state dose"); (3) the 20% to 80% geometries ("6-state dose"); (4) the 10% to 90% geometries ("11-state dose"); (5) the dose distributions for the average phase of the breathing cycle ("ave state" dose). In their study the "11-state dose" is considered the closest representation of a continuous integral over an infinite number of intermediate states between exhale and inhale. The comparison between the "11-state" dose and the cumulative doses estimated by the other scenarios revealed less than 2.5% point dose differences, as illustrated in the color wash displays from Figures 5(a) through 5(d). Such differences represent only a fraction of the changes between the cumulative dose and the static exhale dose, as illustrated in Figure 5(e), and thus are unlikely to have a clinically significant impact on treatment planning metrics such as NTCP or *gEUD*. Interestingly, the time-weighted average breathing phase appears to provide an accurate representation of the actual cumulative dose received over the entire breathing cycle, despite lung deformation and tissue density changes. However, the practicality of using this average geometry is limited due to reproducibility issues. Therefore, using the exhale and inhale geometries appears a more feasible solution for treatment planning. The above-mentioned findings are a consequence of the fact that each voxel dose changes in an approximately linear fashion between exhale and inhale. Further studies are needed to elucidate whether or not the approximation holds well when dealing with tumors that exhibit notable hysteresis (Seppenwoolde et al. 2002). It should also be noted that even if only the exhale and the inhale datasets or simply the average state of the breathing cycle are used to estimate the cumulative dose, the shape of the respiratory pattern is needed in order to evaluate the appropriate exhale/inhale time-weighting factors or to determine the average state during respiration. This, in turn, raises the question of stability/reproducibility of the respiratory motion. It is fairly well established that important changes can occur in the mean tumor position during treatment (Seppenwoolde et al. 2002; Murphy et al. 2002; Kestin et al. 2004; Yan et al. 2005), thus making breathing pattern monitoring an important step in lung cancer treatment. However, the changes in mean tumor position do not invalidate the above conclusions. Instead, this solidifies the fact that breathing should be monitored and if the deviations from the planning scenario are believed to be clinically important, then the new mean position or exhale/inhale weighting factors should be reevaluated and the cumulative dose updated (Rosu et al. 2006).

Image Registration: Where It Matters the Most

The accumulation of doses on the planning CT (computed tomography) is accomplished by using image registration techniques that provide non-rigid body voxel mapping between CT scans acquired over various segments of the ventilatory cycle.

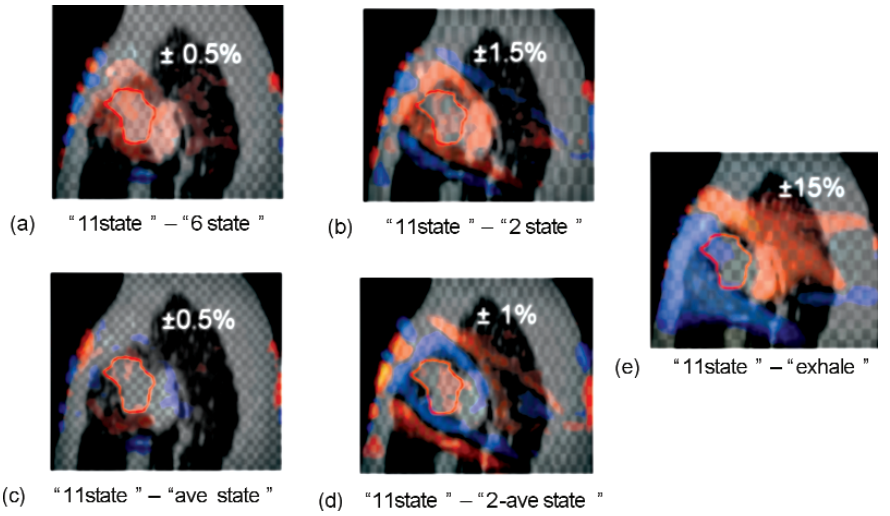

Figure 5.(a)–(d). Dose difference maps between the "11-state" cumulative dose and the cumulative doses estimated by other scenarios; (e) dose difference map between the "11-state" dose and the static exhale dose. Numbers indicated maximum positive (red regions) and negative (blue regions) dose differences.

The most popular registration methods are the spline-based techniques such as the thin-plate spline (TPS) (Schaly et al. 2004; Coselmon et al. 2004) and the B-spline (BPS) (Rietzel et al. 2005; Rosu et al. 2005). Both TPS and BSP require as input a set of control points. However, while in TPS these control points are landmarks manually selected by the user on both datasets that need to be mapped onto each other, the B-spline technique starts with a uniform grid of points distributed across the entire region to be registered. Between the two approaches, B-splines are believed to be more appropriate for describing nonrigid behaviors due to their ability of dealing with local deformations. Each control point belonging to a TPS has a global influence on the transformation and if its position is perturbed, all other points in the transformed image change. By contrast, in B-spline registration perturbing the position of one point only affects the transformation in the neighborhood of that point, thus having a so-called "local support" (Kessler and Roberson 2005).

One approach for quantitatively validating the registration process is to identify landmarks independently of the registration process and to establish how well the registration process brings these landmarks together into alignment. To illustrate this, 14 anatomical landmarks were manually selected on both the exhale and inhale images in places located at secondary bronchi bifurcations, ribs, and spine in places easily identifiable on both datasets for one patient example. These landmarks were different from the 43 landmarks initially used to derive the TPS transformation between the

exhale and inhale datasets. The positions of the inhale landmarks were subsequently calculated by transforming the exhale landmark positions using the registration transformations provided by both the TPS and BSP algorithms. The alignment accuracy was estimated by computing the mean and the standard deviation of the differences between the actual inhale landmark coordinates [along the superior-inferior (SI), anterior-posterior (AP) and left-right (LR) axes] and the corresponding predicted exhale coordinates. The corresponding differences in doses at the actual and predicted landmark positions were also calculated for both the TPS and the BSP techniques. The accuracy of the alignment for both the techniques in each direction was quantified by taking the mean value and the standard deviation of the differences between the predicted and the actual inhale positions for all 14 landmarks. The results are summarized in Table 1. A paired *t*-test performed at 95% confidence level indicated that the differences between the actual and the predicted positions were not significant in any direction, for neither the TPS nor the BSP method. The differences between the landmark positions as predicted by TPS and BSP transformations were also found to be insignificant at the same confidence level. It should also be noted that the differences from Table 1 are smaller than the dose grid size used in this example (3.5 mm).

The differences between the actual and the predicted landmark positions and the corresponding dose differences are shown on Figure 6. The analysis of these plots reveals errors in the registration of landmark points 13 and 14, which were located in the spinal cord, although no motion is expected for these points. The differences in doses were significant (a few Gray magnitude) only for landmarks 8 and 9, which were situated in the high gradient region of the dose distribution. Shown in Figure 7 are the landmark point 9 (secondary bronchi bifurcation), its location with respect to the dose distribution, and the location of its actual and predicted positions on a dose profile. Although both the TPS and the BSP registrations performed similarly for the case analyzed in this study, several interesting features emerged. First, although the two landmarks (13 and 14) located in the spinal cord did not move with breathing, both registration algorithms predicted a few millimeter displacements, indicating that both algorithms are trying to reach a compromise in aligning tissues with different densities (and thus different contrast in the CT images) in order to minimize the overall misalignment. Second, landmarks with rather small displacements (such as landmark 9) underwent large variations in doses. This is explained by the fact that this landmark

Table 1. Mean Values and Standard Deviations of the Differences Between the Predicted and the Actual Inhale Positions for all Landmarks

	Direction					
	RL (x axis)		**AP (y axis)**		**SI (z axis)**	
	TPS	**BSP**	**TPS**	**BSP**	**TPS**	**BSP**
Mean (mm)	0.4	0.8	–1.3	–0.8	0.4	1.0
Standard deviation (mm)	1.8	1.5	2.3	1.7	1.7	1.8

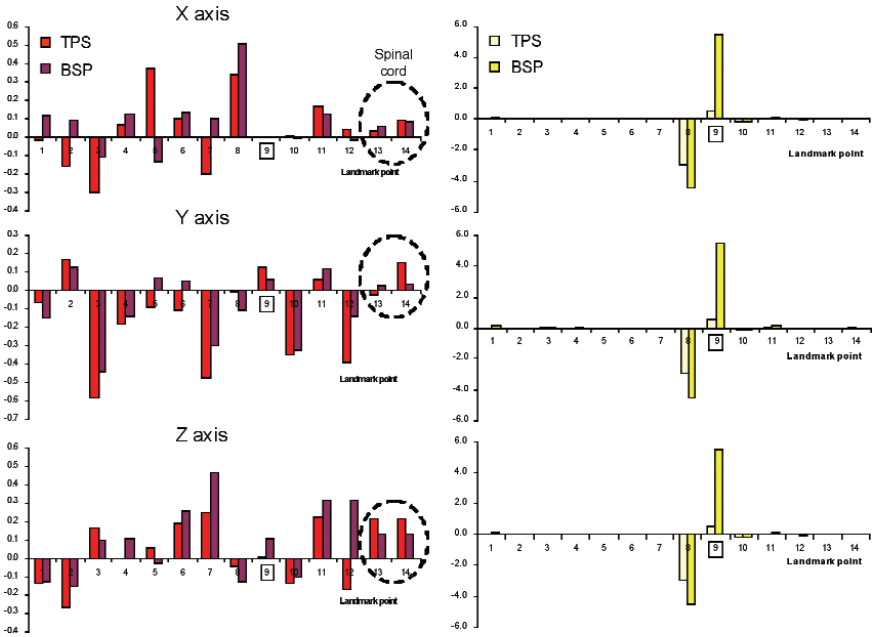

Figure 6. Differences (along x, y, z directions) between the actual and the predicted landmark positions in centimeters (left panel) and the corresponding dose differences in grays (right panel).

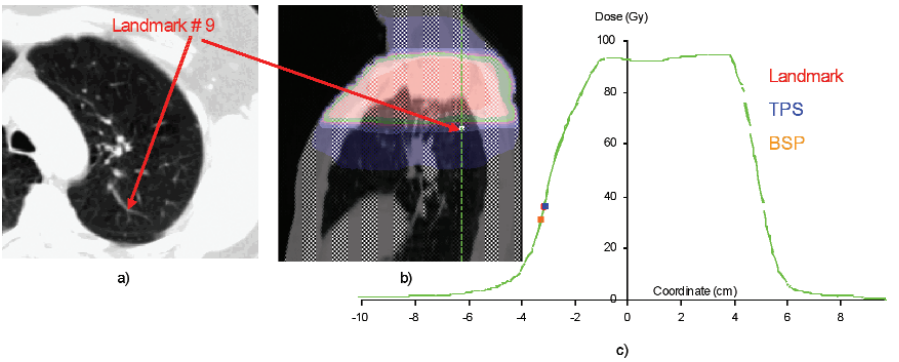

Figure 7. Landmark point 9: (a) location at a secondary bronchi bifurcation shown in axial view; (b) location with respect to the inhale dose distribution; (c) location with respect to the dose profile extracted along the dotted green line.

lies in the gradient region of the dose distribution and thus a few millimeter errors in the position predicted by the registration transformation led to a few Gray errors in predicting the dose received by that landmark point. This suggests that for dosimetric

purposes the registration errors are particularly important in places located in regions where steep dose gradients exist, especially since differences in dose can also arise as a result of deformation and/or motion at these locations.

The example presented above attempts to emphasize the fact that registration errors are clinically important in regions where there are steep dose gradients. The landmark-based evaluation of the registration process as described above seems to be putting BSP and TPS on equal footing, but one should acknowledge the fact that the accuracy of the landmark alignment does not automatically imply similar accuracy everywhere. The B-spline's superiority is at least twofold. First, BSP registration is less user biased, as it starts with a uniform grid of points, as opposed to the TPS approach where control points need to be selected before the registration process is initiated. Second, and perhaps more important, the BSP, unlike TPS, grants a certain degree of "local control."

Motion/Deformation vs. Heterogeneity Effects

While the treatment of lung cancer with radiation poses concerns related to the motion and deformation induced by breathing during treatment delivery, additional issues are raised by the algorithm used for calculating dose distributions, given that many institutions across the country are using dose calculation algorithms that do not correct for tissue heterogeneities, despite the large density variations encountered in the thorax. Therefore, it is perhaps useful to assess how the motion/deformation-induced changes compare with changes induced by tissue inhomogeneities.

Changes in the physical dose either as a result of motion/deformation or variations in tissue densities do certainly exist and can be as large as a few tens of grays. However, for the purpose of radiation therapy, these dose variations, although large, must be assessed in relation to their clinical significance. Moreover, the assessment must be performed separately for tumors and organs at risk, which in turn need to be assessed separately depending on their serial or parallel nature.

One major concern in the lung cancer radiotherapy is radiation-induced pneumonitis, which has been largely related to the mean dose received by the lung (MLD) (Kwa et al. 1998; Seppenwoolde et al. 2003). To date, there are conflicting reports in the literature regarding the importance of heterogeneity corrections (Mah and Van Dyk 1991; Frank et al. 2003), thus further investigation is necessary. As for the deformation effects, it appears that they have a minimal impact on the MLD, largely because the changes induced by the respiratory motion average over a large volume. However, in dose escalation trials, respiratory-induced motion/deformation effects should not be overlooked.

While parallel organs appear less sensitive to motion-induced dose variations, things seem to be different for serial organs, which are sensitive to changes in the maximum dose (Rosu et al. 2005). This is the case for the esophagus, which is often located adjacent to tumors and thus at the beam edge, making this organ susceptible to significant changes in the maximum dose as it moves in and out of the radiation field due to respiration.

To exemplify relative comparisons between heterogeneity and motion-induced effects, several examples are provided here. Figures 8(a) and 8(b) show dose difference displays between the heterogeneous and the homogeneous (i.e., water-like density) calculations in the static case for a patient example in the coronal and sagittal planes, whereas Figure 8(c) shows the difference between the cumulative (over the breathing cycle) and the static dose for the homogeneous calculation. The maximum point dose differences between the heterogeneous and homogeneous calculations are about +10% (though these differences occur at different locations). The *gEUD* evaluation indicates that the heterogeneity effect is dominant for the tumor, with larger values (~2 Gy) in the heterogeneous case, mainly attributed to the decreased attenuation of the primary beam through the lower-density lung tissue when accounting for the inhomogeneities. For the esophagus the motion/deformation effects appear to have a larger impact than the changes in media density. The ventilatory motion brings the esophagus closer to the high-dose area, creating a hot spot that has a strong impact on this organ, due to its serial nature. However, whether the calculation assumes heterogeneous or homogeneous media does not lead to major differences because the density of the esophagus and its vicinity is close to water density in both scenarios. For the normal lung tissue, the effects of motion/deformation are believed to be small. In the example presented in Figure 8, neither the motion nor the heterogeneities has an important impact on changes in the MLD. However, for the example shown in Figure 9, the 80-Gy prescription dose from the heterogeneous calculation would be erroneously escalated to 83 Gy based on the homogeneous dose distribution (to match the lung toxicity from both calculations). This indicates that tissue heterogeneities must be properly accounted for since the dosimetric inaccuracies will likely lead to clinically important differences for tumors, as well as for normal organs. While for rather large field sizes and simple AP/PA beam arrangement heterogeneity effects might not be evident, differences will clearly occur as plans become more conformal, especially when non-

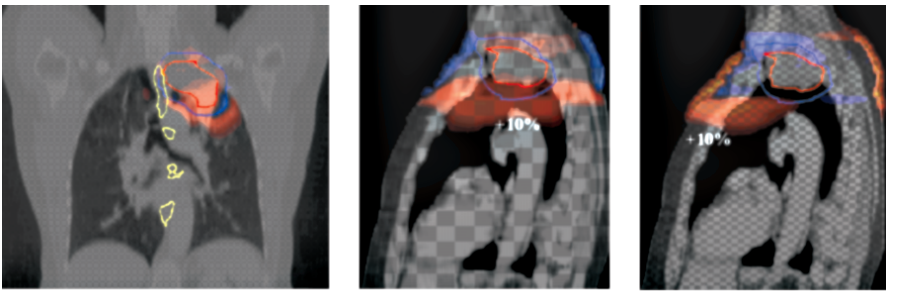

Figure 8. Dose difference displays between the heterogeneous and homogeneous dose calculations in (a) coronal and (b) sagittal views; (c) Dose difference between the cumulative and static dose distribution in the homogeneous media. The contours are as follows: red: CTV, blue: PTV, and yellow: esophagus. The beam energy is 6 MV. Red and blue regions indicate positive and respectively negative dose differences.

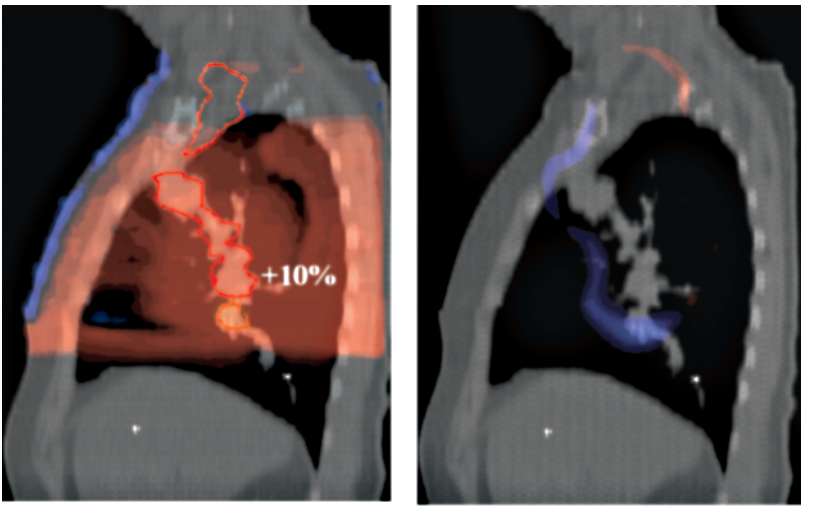

Figure 9. (a) Dose difference display between the heterogeneous and homogeneous dose calculations in the static case; (b) dose difference display between the cumulative and static dose distribution and heterogeneous media (CTV shown in red). The beam energy is 6 MV. Red and blue regions indicate positive and respectively negative dose differences.

coplanar beams are used, or when treating small lesions embedded in low-density lung tissue. We should also note that as the dose increases, the dose-response curves become steeper and more sensitive to small variations. Moreover, the data used to describe the lung response to radiation are highly uncertain, and the refinement of such data cannot take place unless we correlate the occurrence of complications with accurate doses.

Conclusions

Recent advances in CT imaging, image registration techniques, and dose calculation algorithms are great assets in the continuous effort of improving, prior to treatment, the accuracy of the dose distribution. This is of major importance in lung cancer, for which radiation therapy is an integral part of the medical care. Unfortunately, the rate of tumor control is far from satisfactory and some believe that to achieve better response rates in lung cancer, dose escalation is needed. However, this is limited by the adverse effect radiation has on the healthy lung tissue, and therefore it is necessary to try to achieve a higher degree of conformality of the dose to tumor to spare the normal tissues. Respiratory motion, however, may be hampering these efforts. Techniques such as deep inspiration and breath hold can certainly benefit the patient, but they are not suitable for all patients; therefore, it is important to evaluate what are the true dosimetric consequences of delivering radiation treatments during free breathing.

In this chapter, we have reviewed some basic aspects related to the treatment planning when multiple datasets are available. We have learned that deformation effects in the thorax appear to be small for both the tumors [if the planning target volume (PTV) is properly designed] and the normal lung tissue (due to an averaging effect of the changes in dose over a parallel organ of large volume). However, special care should be taken when serial organs are involved (such as the esophagus), especially when such structures are located adjacent to the target. Despite the large amount of deformation that occurs in the thorax, our study indicates that CT scans representative for as many as two phases of the ventilatory cycle (exhale and inhale, which have the highest probability of occurrence) are sufficient to predict cumulative doses accurately. Even one dataset acquired at the average phase of the breathing cycle would suffice, but this may be hard to acquire due to reduced reproducibility.

The methods presented here will have to be used on a large scale in daily planning before their clinical benefit can be proven. Also, it is possible that these more accurate means of estimating the doses received by patients will eventually improve our understanding of the tissue response to radiation. Another reason for dealing with motion/deformation effects prior to treatment is to be able to overcome the issues associated with PTV-based planning. Future studies will need to investigate how much margin reduction is achievable without compromising the tumor control and what the clinical implications are for normal tissues.

Last, but not least, we have to note that in 4-D planning we are facing a new class of uncertainties associated with 4-D CT scan artifacts, deformable registration, motion reproducibility, and multileaf collimator (MLC) positional and temporal accuracy in dynamic deliveries. And, as pointed out by Keall et al. (2005), the cumulative effects of such uncertainties need to be significantly smaller than the cumulative uncertainties encountered in 3-D planning in order to make 4-D planning a viable option and thereby to justify the additional workload involved.

Acknowledgment

This work has been supported in part by National Institutes of Health (NIH) [National Cancer Institute (NCI)] grants: R01 CA106770 and P01 CA59827.

References

Austin-Seymour, M., I. Kalet, J. McDonald, S. Kromhout-Schiro, J. Jacky, S. Hummel, and J. Unger. (1995). "Three dimensional planning target volumes: a model and a software tool." *Int J Radiat Oncol Biol Phys* 33:1073–1080.

Balter, J. M., R. K. Ten Haken, T. S. Lawrence, K. L. Lam, and J. M. Robertson. (1999). "Uncertainties in CT-based radiation therapy treatment planning associated with patient breathing." *Int J Radiat Oncol Biol Phys* 36:167–174.

Bookstein, F. L. (1989). "Principal warps: Thin-plate splines and the decomposition of deformations." *IEEE Trans Pattern Anal Mach Intell* 11:567–585.

Brock, K. K., D. L. McShan, R. K. Ten Haken, S. J. Hollister, L. A. Dawson, and J. M. Balter. (2003). "Inclusion of organ deformation in dose calculations." *Med Phys* 30:290-295.

Chetty, I. J., P. M. Charland, N. Tyagi, D. L. McShan, B. A. Fraass, and A. F. Bielajew. (2003). "Photon beam relative dose validation of the DPM Monte Carlo code in lung-equivalent media." *Med Phys* 30:563–573.

Coselmon, M. M., J. M. Balter, D. L. McShan, and M. L. Kessler. (2004). "Mutual information based CT registration of the lung at exhale and inhale breathing states using thin-plate splines." *Med Phys* 31:2942–2948.

Dawson, L. A., K. K. Brock, S. Kazanjian, D. Fitch, C. J. McGinn, T. S. Lawrence, R. K. Ten Haken, and J. Balter. (2001). "The reproducibility of organ position using active breathing control (ABC) during liver radiotherapy." *Int J Radiat Oncol Biol Phys* 51:1410–1421.

Foskey, M., B. Davis, L. Goyal, S. Chang, E. Chaney, N. Strehl, S. Tomei, J. Rosenman, and S. Joshi. (2005). "Large deformation three-dimensional image registration in image-guided radiation therapy." *Phys Med Biol* 50:5869–5892.

Fraass, B. A. "The development of conformal radiation therapy." *Med Phys* 22:1911–1921.

Frank, S. J., K. M. Forster, C. W. Stevens, J. D. Cox, R. Komaki, Z. Liao, S. Tucker, X. Wang, R. E. Steadham, C. Brooks, and G. Starkschall. (2003). "Treatment planning for lung cancer: Traditional homogeneous point-dose prescription compared with heterogeneity-corrected dose-volume prescription." *Int J Radiat Oncol Biol Phys* 56:1308–1318.

Hanley, J., M. M. Debois, D. Mah, G. S. Mageras, A. Raben, K. Rosenzweig, B. Mychalczak, L. H. Schwartz, P. J. Gloeggler, W. Lutz, C. C. Ling, S. A. Leibel, Z. Fuks, and G. J. Kutcher. (1999). "Deep inspiration breath-hold technique for lung tumors: The potential value of target immobilization and reduced lung density in dose escalation." *Int J Radiat Oncol Biol Phys* 45:603–611.

Heath, E., and J. Seuntjens. (2006). "A direct voxel tracking method for four-dimensional Monte Carlo dose calculations in deforming anatomy." *Med Phys* 33:434–445.

Keall, P. J., J. V. Siebers, S. Joshi, and R. Mohan. (2004). "Monte Carlo as four-dimensional radiotherapy treatment-planning tool to account for respiratory motion." *Phys Med Biol* 49:3639–3648.

Keall, P. J., S. Joshi, S. S. Vedam, J. V. Siebers, V. R. Kini, and R. Mohan. (2005). "Four-dimensional radiotherapy planning for DMLC-based respiratory motion tracking." *Med Phys* 32:942–951.

Ketting, C. H., M. Austin-Seymour, I. Kalet, J. Unger, S. Hummel, J. Jacky. (1997). "Consistency of three-dimensional planning target volumes across physicians and institutions." *Int J Radiat Oncol Biol Phys* 37:445–453.

Kessler, M. L., and M. Roberson. "Image Registration and Data Fusion for Radiotherapy Treatment Planning" in *New Technologies in Radiation*. W. Schlegel, T. Bortfeld, and A. L. Grosu (Eds.). New York: Springer-Verlag, 2005.

Kessler, M. L., M. Roberson, R. Zeng, and J. Fessler. (2004). "Deformable image registration using multiresolution b-splines." *Med Phys* 31:1792.

Kestin, L., C. Vargas, G. Hugo, J. Liang, D. Letourneau, J. Wong, and D. Yan. (2004). "Breathing variation during thoracic radiations for adaptive radiotherapy of lung cancer." *Int J Radiat Oncol Biol Phys* 60:S610 (Abstract).

Kwa, S. L., J. C. Theuws, A. Wagenaar, E. M. Damen, L. J. Boersma, P. Baas, S. M. Muller, and J. V. Lebesque. (1998). "Radiation pneumonitis as a function of mean lung dose: An analysis of pooled data of 540 patients." *Int J Radiat Oncol Biol Phys* 42:1–9.

Low, D. A., M. Nystrom, E. Kalinin, P. Parikh, J. F. Dempsey, J. D. Bradley, S. Mutic, S. H. Wahab, T. Islam, G. Christensen, D. G. Politte, and B. R. Whiting. (2003). "A method for the reconstruction of four-dimensional synchronized CT scans acquired during free breathing." *Med Phys* 30:1254–1263.

Mah, K., and J. Van Dyk. (1991). "On the impact of tissue inhomogeneity corrections in clinical thoracic radiation therapy." *Int J Radiat Oncol Biol Phys* 21:1257–1267.

Mah, D., J. Hanley, K. E. Rosenzweig, E. Yorke, L. Braban, C. C. Ling, S. A. Leibel, and G. Mageras. (2000). "Technical aspects of the deep inspiration breath-hold technique in the treatment of thoracic cancer." *Int J Radiat Oncol Biol Phys* 48:1175–1185.

Mazonakis, M., J. Damilakis, H. Varveris, P. Prassopoulos, and N. Gourtsoyiannis. (2001). "Image segmentation in treatment planning for prostate cancer using the region growing technique." *Br J Radiol* 74:243–248.

Murphy, M. J., D. Martin, R. Whyte, J. Hai, C. Ozhasoglu, and Q. T. Le. (2002). "The effectiveness of breath-holding to stabilize lung and pancreas tumors during radiosurgery." *Int J Radiat Oncol Biol Phys* 53:475–482.

Pan, T., T.-Y. Lee, E. Rietzel, and G. T. Chen. (2004). "4D-CT imaging of a volume influenced by respiratory motion on multi-slice CT." *Med Phys* 31:333–340.

Rietzel, E., G. T. Chen, N. C. Choi, and C. G. Willet. (2005). "Four-dimensional image-based treatment planning: Target volume segmentation and dose calculation in the presence of respiratory motion." *Int J Radiat Oncol Biol Phys* 61:1535–1550.

Rosenzweig, K. E., J. Hanley, D. Mah, G. Mageras, M. Hunt, S. Toner, C. Burman, C. C. Ling, B. Mychalczak, Z. Fuks, S. A. Leibel. (2000). "The deep inspiration breath-hold technique in the treatment of inoperable non-small-cell lung cancer." *Int J Radiat Oncol Biol Phys* 48:81–87.

Rosu, M., I. J. Chetty, J. M. Balter, M. L. Kessler, D. L. McShan, and R. K. Ten Haken. (2005). "Dose reconstruction in deforming lung anatomy: Dose grid size effects and clinical implications." *Med Phys* 32:2487–2495.

Rosu, M., J. M. Balter, I. J. Chetty, M. L. Kessler, D. L. McShan, and R. K. Ten Haken. (2006). "How extensive of a 4D dataset is needed for lung cancer treatment planning? A simulation study." *Med Phys* (Submitted).

Rueckert, D., L. I. Sonoda, C. Hayes, D. L. Hill, M. O. Leach, and D. J. Hawkes. (1999). "Nonrigid registration using free-form deformations: Application to breast MR images." *IEEE Trans Med Imag* 18:712–721.

Schaly, B., J. A. Kempe, G. S. Bauman, J. J. Battista, and J. Van Dyk. (2004). "Tracking the dose distribution in radiation therapy by accounting for variable anatomy." *Phys Med Biol* 49:791–805.

Seppenwoolde, Y., H. Shirato, K. Kitamura, S. Shimizu, M. van Herk, J. V. Lebesque, and K. Miyasaka. (2002). "Precise and real-time measurement of 3D tumor motion in lung due to breathing and heartbeat, measured during radiotherapy." *Int J Radiat Oncol Biol Phys* 53:822–834.

Seppenwoolde, Y., J. V. Lebesque, K. de Jaeger, J. S. Belderbos, L. J. Boersma, C. Schilstra, G. T. Henning, J. A. Hayman, M. K. Martel, and R. K. Ten Haken. (2003). "Comparing different NTCP models that predict the incidence of radiation pneumonitis." *Int J Radiat Oncol Biol Phys* 55:724–735.

Shimizu, S., H. Shirato, K. Kagei, T. Nishioka, X. Bo, H. Dosaka-Akita, S. Hashimoto, H. Aoyama, K. Tsuchiya, and K. Miyasaka. (2000). "Impact of respiratory movement on the computed tomographic images of small lung tumors in three-dimensional (3D) radiotherapy." *Int J Radiat Oncol Biol Phys* 46:1127–1133.

van Herk, M. and H. M. Kooy. (1994). "Automatic three-dimensional correlation of CT-CT, CT-MRI, and CT-SPECT using chamfer matching." *Med Phys* 21:1163–1178.

Vedam, S. S., P. J. Keall, V. R. Kini, H. Mostafavi, H. P. Shukla, and R. Mohan. (2003). "Acquiring a four-dimensional computed tomography dataset using an external respiratory signal." *Phys Med Biol* 48:45–62.

Violla, P. A., and W. M. Welles. "Alignment by Maximization of Mutual Information" in P*roceedings of the Fifth International Conference on Computer Vision*, IEEE95CH35744, pp. 16–23, 1995.

Wong, J. W., M. B. Sharpe, D. A. Jaffray, V. R. Kini, J. M. Robertson, J. S. Stromberg, and A. A. Martinez. (1999). "The use of active breathing control (ABC) to reduce margin for breathing motion." *Int J Radiat Oncol Biol Phys* 44:911–999.

Yan, D., D. Lockman, A. Martinez, J. Wong, D. Brabbins, F. Vicini, J. Liang, and L. Kestin. (2005). "Computed tomography guided management of interfractional patient variation." *Radiat Oncol* 15:168–179.